Special Collection

XAS and EPR in Situ Observation of Ru(V) Oxo Intermediate in a Ru Water Oxidation Complex**

Natalia Levin,*[a] Carla Casadevall,[b, d] George E. Cutsail, III,[a, c] Julio Lloret-Fillol,*[b] Serena DeBeer,[a] and Olaf Rüdiger*[a]

In this study, we combine in situ spectroelectrochemistry coupled with electron paramagnetic resonance (EPR) and X-ray absorption spectroscopies (XAS) to investigate a molecular Ru-based water oxidation catalyst bearing a polypyridinic backbone $[Ru^{II}(OH_2)(Py_2Metacn)]^{2+}$. Although high valent key intermediate species arising in catalytic cycles of this family of compounds have remain elusive due to the lack of additional anionic ligands that could potentially stabilize them, mechanistic studies performed on this system proposed a water nucleophilic attack (WNA) mechanism for the O–O bond formation. Employing *in situ* experimental conditions and complementary spectroscopic techniques allowed to observe intermediates that provide support for a WNA mechanism, including for the first time a Ru(V) oxo intermediate based on the **Py_2Metacn** ligand, in agreement with the previously proposed mechanism.

In the quest for feasible renewable energy schemes, the "hydrogen economy" offers an attractive solution,[1] where H_2 and O_2 can be produced through water electrolysis (Eqs. 1, 2), employing the intermittent energy surplus arising from renewable energies. These two species can later on be recombined in fuel cells to afford a green energy source at any required moment, releasing only water and steam as by-products.[2] The water splitting reaction is complex and requires the use of catalysts to make it feasible. In particular, the water oxidation (WO) half-reaction, requiring 4 electron transfer steps remains the most challenging reaction, and to date, most homogeneous WO catalysts (WOC) operate at moderate overpotentials. Over three decades ago, the first well-characterized synthetic WOC was reported: the Ru-based "blue-dimer" (BD).[3] Since then, important effort has been put in the development of new homogenous catalysts, but guidelines for predictive rational design to improve WOCs are still insufficiently developed. The WOCs are typically complexes based on transition metals that help reduce the energy barrier for the process. The first critical step involves the formation of a high-valent metal-oxo species that arises from the subsequent oxidation of an aquo complex. Then, this oxo species can follow two major mechanisms: water nucleophilic attack (WNA) where a second water molecule attacks the electrophilic high-valent M-oxo species or intramolecular radical coupling of two M-oxyl units (I2 M) where the new O–O bond comes from the radical coupling between two equal species.[4]

$$2H_2O \rightarrow O_2 + 4H^+ + 4e^- \quad (1)$$

$$2H^+ + 2e^- \rightarrow H_2 \quad (2)$$

Continuing on the path of the BD, many Ru-based complexes have appeared as good WOCs, showing stability and high efficiency.[5] Even if a lot of interest is directed to the use of less expensive, earth abundant metals as catalysts, the high efficiency and especially the stability of Ru species is still to be surpassed.[6] Additionally, the complexity of the WO reaction, due to the multiple bond breaking and forming processes that take place during its mechanism, requires the involvement of multiple intermediates. In this regard, spectroscopic techniques are of special interest, and particularly in situ/operando techniques, where the catalyst and its intermediate species are characterized while performing the desired reaction.

Among Ru-based WOCs, owing to the ligand stability towards oxidation and its versatility for symmetric and non-symmetric functionalization,[7] catalysts based on the macrocyclic 1,4,7-triazacyclononane (tacn) are very interesting for the study of the WO reaction.[8] The catalyst $[Ru^{II}(OH_2)(Py_2{}^{Me}tacn)]^{2+}$

[a] Dr. N. Levin, Dr. G. E. Cutsail, III, Prof. S. DeBeer, Dr. O. Rüdiger
Max Planck Institute for Chemical Energy Conversion
Stiftstr. 34–36, D-45470 Mülheim an der Ruhr,
Germany
E-mail: natalia.levin@cec.mpg.de
olaf.ruediger@cec.mpg.de
[b] Dr. C. Casadevall, Prof. J. Lloret-Fillol
Institute of Chemical Research of Catalonia (ICIQ)
Avinguda Països Catalans, 16, 43007,
Tarragona, Spain
E-mail: jlloret@iciq.es
[c] Dr. G. E. Cutsail, III
University of Duisburg-Essen
Department of Chemistry
Universitätstr. 7, D-45141 Essen,
Germany
[d] Dr. C. Casadevall
Current address:
Department of Chemistry
University of Cambridge
Lensfield road, CB2 1EW,
Cambridge, UK.

[**] XAS: X-ray Absorption Spectroscopy; EPR: Electron Paramagnetic Resonance

Supporting information for this article is available on the WWW under https://doi.org/10.1002/celc.202101271

Special Collection An invited contribution to the Wolfgang Schuhmann Festschrift

, reported by the group of Lloret-Fillol is a mononuclear Ru-WOC bearing a tacn-derived backbone.[8c] The starting compound and further species arising in the catalytic cycle **[Ru^{III}(OH)(Py$_2$^{Me}tacn)]$^{2+}$** and **[Ru^{IV}(O)(Py$_2$^{Me}tacn)]$^{2+}$** were characterized by different spectroscopic techniques, UV-vis spectroelectrochemistry, Cryo-spray high-resolution mass spectrometry (CSI-HRMS) and a complete Pourbaix diagram for the species was obtained.[8c] DFT calculations together with ^{18}O-labelling and kinetic studies pointed towards a WNA mechanism.

Using an isolated **[Ru^{IV}(O)(Py$_2$^{Me}tacn)]$^{2+}$** as a starting material, a Ru(IV) side-on peroxo species (**^{2}η-Ru^{IV}(O–O)**) was isolated as an intermediate after the rate determining step in the WNA mechanism),[9] In the same work, a **[Ru^{V}(O)(Py$_2$^{Me}tacn)]$^{3+}$** was proposed as the species responsible for the O–O bond formation via WNA (Figure S1).

With the aim of characterizing the proposed active species of the catalytic cycle, a detailed experimental and theoretical investigation of the well-defined monomeric catalyst **[Ru^{II}(OH$_2$)(Py$_2$^{Me}tacn)]$^{2+}$** is presented. Owing to its rather slow catalytic performance (TOF 4.10^{-3} s^{-1}),[8c] **[Ru^{II}(OH$_2$)(Py$_2$^{Me}tacn)]$^{2+}$** is an ideal platform to trap intermediate species. These experiments allow us to understand the electronic structure of the catalytic intermediates and will therefore pave a path for controlling the reaction's mechanism and designing tailor-made WOCs based on earth-abundant metals.

Herein, a study with complementary *in situ* Electron Paramagnetic Resonance (EPR) and X-ray Absorption Spectroscopy (XAS) is presented. EPR spectroscopy is often used to study WOCs and intermediates within a catalytic cycle that alternate between EPR active and inactive spin-states. Ru^{III} species show EPR signals arising from a S = 1/2 spin center with anisotropic g-values and have been detected in ex situ experiments for monomeric[9–10] and dimeric catalysts.[11] However, EPR spectra of more elusive Ru^{V} species, regardless of being related to WOCs or not, have been reported for fewer monomeric[10a,e–i,12] or dimeric species.[11b,c,13] XAS measurements complement EPR, since the former, owing to its element-selective properties, offer unique insight into the geometric and electronic structures of all Ru-based species (both EPR active and inactive).[10a–c,11b]

In order to facilitate intermediate trapping, we designed an EPR spectroelectrochemical (SEC) electrolysis cell built around a Quartz EPR-tube that can be completely frozen during an applied potential (Figure S2). The most extended type of spectroelectrochemical *in situ* EPR cells use a flow scheme and are used to monitor the electrochemical formation of organic radicals, which can be performed at room[14] or elevated temperatures.[15] The study of transition-metal paramagnetic species requires low-temperature EPR measurements to slow the fast relaxation of the unpaired electrons. Therefore, for transition metals, EPR electrochemical titrations are usually performed by *ex situ* electrolysis, taking samples at different applied potentials and freezing them, requiring usually larger volumes of sample and sample transfer operations that may hinder detection of unstable species. Our newly designed cell operates with very limited volume (250 µL), avoids clogging issues that could result from freezing/thawing a flow system and may be used not only for X-band but also for Q-band or pulsed measurements. Our first aim was to validate the cell by running SEC in aqueous solutions and compare the results with samples prepared in a traditional two-compartment electrolysis cell. We prepared a 2 mM solution of **[Ru^{II}(OH$_2$)(Py$_2$^{Me}tacn)]$^{2+}$** and applied different potentials based on previous electrochemical measurements.[8c] At 0 V *vs* Ag/AgCl/KCl sat., the EPR showed almost a clean background, as expected for a Ru^{II}(OH) complex (Figure 1, left, top spectrum). Upon oxidation at 0.5 V a rhombic signal appears with anisotropic g-values and resolved hyperfine coupling along g_3 from the ^{99}Ru (12.7% natural abundance, n.a.) and ^{101}Ru (17.0% n.a.) isotopes, each having *I* =

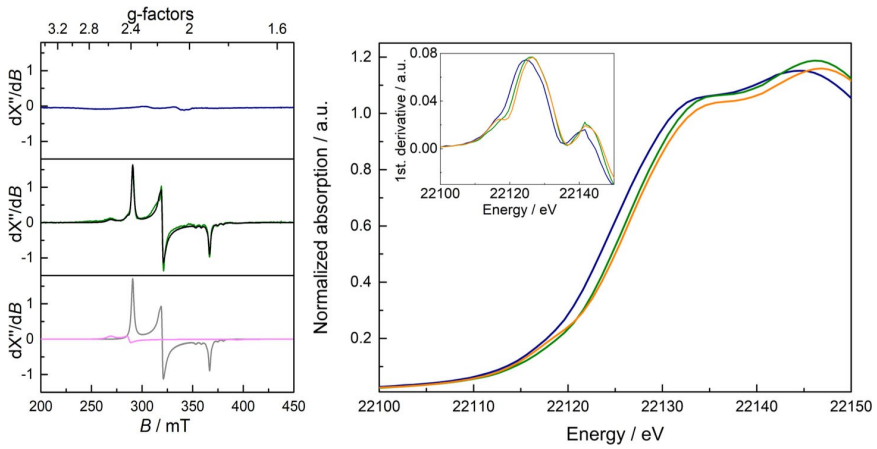

Figure 1. Left: X-band *in situ* EPR spectra of **[Ru^{II}(OH$_2$)(Py$_2$^{Me}tacn)]$^{2+}$** in aqueous solution: phosphates buffer 0.1 M/NaOTf 2 M, pH 7.2 at 10 K. Measured in the *in situ* EPR electrochemical cell under 0 V (top panel, blue spectrum) and under 0.5 V (middle panel: experimental spectrum (green, background corrected with the blue spectrum under 0 V) and simulated spectrum (black)). Bottom panel: components present in the simulation of the green spectrum. Major component (grey) accounts for 87% of the intensity (g = [2.386, 2.168, 1.892], A = [5.2, 9.6, 48]/10^{-4} cm^{-1}, W = [1.76, 0.105, 16.7] G). Minor component (pink) accounts for 13% of the intensity (g = [2.582, 2.417, 1.760], W = [50.5, 17.2, 57.0] G). **Right**: Ru K-edge XAS spectra of **[Ru^{II}(OH$_2$)(Py$_2$^{Me}tacn)]$^{2+}$** in aqueous solution: phosphates buffer 0.1 M/NaOTf 1 M. Freeze-quenched samples prepared in a UV-vis electrochemical cell under different potentials: 0 V (blue), 0.5 V (green), 1.3 V (orange). Inset: First derivative of the Ru K-edge XAS spectra. All reported redox potentials are referred to Ag/AgCl, KCl sat.

5/2 nuclear spin (Figure 1, left, middle spectrum). There is also a 13% component of a species exhibiting a broader EPR spectrum, as reported elsewhere for another WOC and attributed to a small amount of an intermediate species with a distorted ligand environment.[10d] Further increase of the potential to 1.3 V results in the reduction of the EPR signal as the sample is further oxidized to the EPR silent Ru(IV) form (not shown). These results were undistinguishable to the spectra obtained ex situ (Figures S3 and S4) and in agreement with UV-Vis observations. In parallel to the EPR experiments, the *ex situ* samples were also freeze-quenched and X-ray K-edge absorption spectroscopy was collected at a synchrotron light source. The XANES Ru K-edge spectra (Figure 1, right) show a small shift of the rising edge to higher energies as the applied potential is increased subsequently from 0 to 0.5 and 1.3 V (*vs* Ag/AgCl/KCl sat.), in agreement with the increment in the oxidation state of the metal. This shift is more evident on the first derivative plot in Figure 1 (right, inset), where the appearance of a feature in the pre-edge region at 22116 eV is also visible. The pre-edge transitions correspond to dipole forbidden 1 s to 4d transitions that upon mixing with the 2p orbitals of the ligands become partially allowed. As the complex is oxidized to Ru(IV) oxo, the 2p orbitals of the O overlap more strongly with the 4d orbitals and the intensity of the pre-edge increases.[10h] The calculated spectra using TD-DFT agree with these observations and allow us to confirm the orbital origin of the pre-edge feature for the more oxidized species (Figure S5). Ru K-edge EXAFS was collected and is shown in Figure S6. Data analysis indicate shortening of the Ru–O distance upon increase of the oxidation state and is in agreement with DFT optimized structures (1.78 vs 1.80 Å, respectively, Table S1).

Similarly to what we did for the spectroelectrochemical EPR cell, we designed an *in situ* XAS-electrolysis cell. We built a thin-layer flow cell for electrolysis that could be used while simultaneously collecting XAS in fluorescence mode (Figure S9). We could reproduce under *in situ* conditions the results measured *ex situ* (not shown) with potential equilibration times around 20 min.

In acidic aqueous solutions, we could not detect any species compatible with an oxidation state higher than 4+, both using EPR or XAS spectroelectrochemical cells, when starting from **$[Ru^{III}(OH)(Py_2^{Me}tacn)]^{2+}$**. To investigate if a Ru(V) could be part of the catalytic cycle, we repeated the SEC experiments using isolated **$[Ru^{IV}(O)(Py_2^{Me}tacn)]^{2+}$**[9] in dry organic solvent. Prior to the SEC experiment a square wave voltammetry (SWV) was recorded to select the applied potentials. Two small peaks can be identified in the SWV at 1 V and a faint one at 1.5 V (Figure 2), in agreement with previous studies.[9] For the EPR experiment, the electrolysis was carried out at −50 °C inside a N_2 atmosphere glovebox using butyronitrile as solvent. The as-dissolved compound did not exhibit any prominent spectral feature, owing to the EPR-silent Ru(IV) state, with just a small signal from Ru(III) species (Figure 2, left, top spectrum). After applying a constant potential for 10 minutes, the sample was rapidly frozen at applied potential. At +1.5 V (*vs* Ag/AgCl/KCl sat.), the EPR measurements shows a new signal (Figures 2 left and S11) with a prominent positive peak at 265 mT and a zero-crossing feature at 295 mT. These two features are assigned as the g_1 and g_2 features of a new rhombic EPR spectrum where g_3 is broad and not observed at higher fields. This spectrum may be simulated as an anisotropic $S = {}^1/_2$ spin (Figure 2 left). This new $S = {}^1/_2$ EPR signal is generated at higher potentials than the $S = 0$, d^4 Ru(IV) starting material (Figure 2, top left). This signal can be reproduced while cycling back and for between 1.2 and 1.5 V, indicating reversibility in the process. The new half-integer spin species indicates a one-electron oxidation and the broad EPR spectrum and large g-shifts suggest the unpaired electron is Ru-centered due the large spin-orbit coupling of Ru. Parallel *in-situ* XAS studies (below) suggest the Ru center is oxidized. The new EPR signal is therefore most consistent with a Ru(V) oxidation state and accounts for 92% conversion of the relative integration of the Ru(III) $S = {}^1/_2$ species.

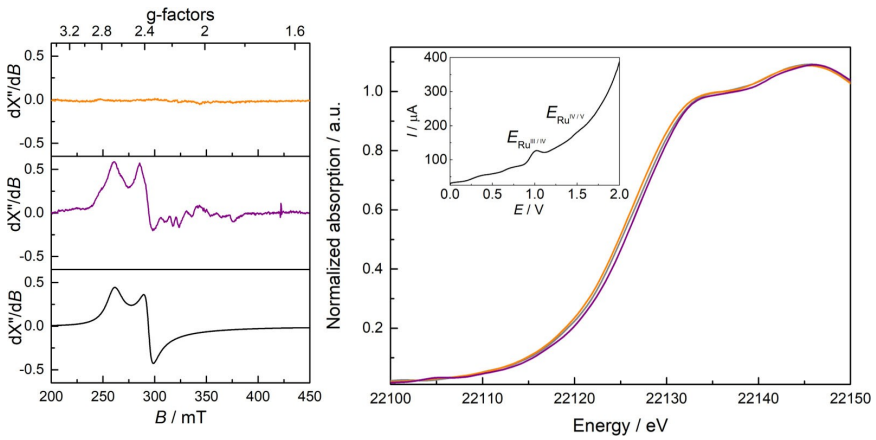

Figure 2. Left: X-band *in situ* EPR spectrum of **$[Ru^{IV}(O)(Py_2^{Me}tacn)]^{2+}$** in dry butyronitrile $TBAPF_6$ 0.3 M measured at 25 K in the *in situ* EPR electrochemical cell under 1.1 V (top, orange spectrum) and under 1.5 V (middle, purple spectrum). Bottom spectrum: simulated spectrum (black) of the middle spectrum ($g = [2.67, 2.37]$, g_3 not resolved). Right: Ru K-edge XAS spectra of **$[Ru^{IV}(O)(Py_2^{Me}tacn)]^{2+}$** in dry acetonitrile $TBAPF_6$ 0.1 M measured in the *in situ* X-ray electrochemical cell under increasing potentials: 1.1 V (orange), 1.7 V (grey), 2.0 V (purple). Inset: SWV voltammogram of $[Ru^{IV}(O)(Py_2^{Me}tacn)]^{2+}$ in dry acetonitrile $TBAPF_6$ 0.1 M measured in the *in situ* X-ray electrochemical cell. All reported redox potentials are referred to Ag/AgCl, KCl sat.

XAS experiments present additional challenges such as long scan times (several minutes) and room temperature restricted *in situ* measurements. To overcome these limitations we used the QEXAFS setup at SuperXAS beamline at SLS. By doing so, we collected 600 spectra during a 10 min exposure time, after which we exposed the beam to fresh solution. Room-temperature measurements did not yield changes in the XAS measurements, probably as a result of the instability of high-valent ruthenium under the intense photon flux of the experiment. Freezing of the sample during acquisition with liquid nitrogen stream was necessary to observe shifts of the XAS edges. The Ru K-edge XAS data (Figure 2, right) shows an increase in the rising edge as the applied potential is increased, which is consistent with the formation of high-valent Ru species.

In summary, we have shown how *in situ* spectroelectrochemistry can be employed to trap and characterize extremely reactive intermediate species. By applying the appropriate redox potential we have demonstrated that we can quantitatively transform the $[Ru^{II}(OH_2)(Py_2^{Me}tacn)]^{2+}$ into its corresponding Ru(III) EPR-active form. Further oxidation shifted the Ru K-edge to higher energy, and produced an EPR silent state, in agreement with the formation of the Ru(IV) oxo complex. Oxidation of the Ru(IV) oxo complex in dry organic solvent showed a further increase of the Ru K-edge to higher energy, indicating that this mononuclear Ru(IV)=O complex could be further oxidized. The new EPR signature is most consistent as a Ru(V). This work shows that combination of electrochemistry with *in situ* spectroscopy can help to capture catalytic intermediates and provide the foundation to understand how electrocatalysts work.

Acknowledgements

We acknowledge the Paul Scherrer Institut, Villigen, Switzerland for provision of synchrotron radiation beamtime at beamline SuperXAS of the SLS and would like to thank Dr. Maarten Nachtegaal for assistance. Stanford Synchrotron Radiation Lightsoursce (SLAC) is also acknowledged for the allocation of beamtime at beamline SSRL 9–3, where ex-situ Ru K-edge measurements were performed. Use of the SLAC National Accelerator Laboratory is supported by the U.S. Department of Energy, Office of Science, Office of Basic Energy Sciences under Contract No. DE-AC02-76SF00515. Casey Van Stappen, Anselm Hahn, Karolina Lewandowska and Albert Thor Thorhallsson are thanked for their assistance during XAS measurements. NL, GC, SD and OR thank the Max-Planck-Society for funding. JL and CC thank the ICIQ Foundation, MEC for a Ph.D. grant FPU14/02550 (C.C.), European Research Foundation for project FP7-PEOPLE-2010-ERG-268445 (J.L.-F.), the MICINN through Severo Ochoa Excellence Accreditation 2020- 2023 (CEX2019-000925-S, MIC/AEI) and MICINN (PID2019-110050RB-I00, J.L-F.). We acknowledge Catexcel for a generous donation of Ts3tacn. The authors thank Leonid Rapatskiy, Thomas Weyhermüller and Christoph Laurich for technical assistance. Open Access funding enabled and organized by Projekt DEAL.

Conflict of Interest

The authors declare no conflict of interest.

Keywords: spectroelectrochemistry · water oxidation · ruthenium · catalyst · in situ electrochemistry

[1] L. Barreto, A. Makihira, K. Riahi, *Int. J. Hydrogen Energy* **2003**, *28*, 267–284.
[2] J. D. Blakemore, R. H. Crabtree, G. W. Brudvig, *Chem. Rev.* **2015**, *115*, 12974–13005.
[3] a) S. Berardi, S. Drouet, L. Francàs, C. Gimbert-Suriñach, M. Guttentag, C. Richmond, T. Stoll, A. Llobet, *Chem. Soc. Rev.* **2014**, *43*, 7501–7519; b) S. W. Gersten, G. J. Samuels, T. J. Meyer, *J. Am. Chem. Soc.* **1982**, *104*, 4029–4030.
[4] J. Kamdar, D. Grotjahn, *Molecules* **2019**, *24*, 494–494.
[5] J. J. Concepcion, J. W. Jurss, M. K. Brennaman, P. G. Hoertz, A. O. T. Patrocinio, N. Y. Murakami Iha, J. L. Templeton, T. J. Meyer, *Acc. Chem. Res.* **2009**, *42*, 1954–1965.
[6] M. D. Kärkäs, O. Verho, E. V. Johnston, B. Åkermark, *Chem. Rev.* **2014**, *114*, 11863–12001.
[7] E. Macedi, A. Bencini, C. Caltagirone, V. Lippolis, *Coord. Chem. Rev.* **2020**, *407*, 213151–213151.
[8] a) M. Yoshida, S. Masaoka, J. Abe, K. Sakai, *Chem. Asian J.* **2010**, *5*, 2369–2378; b) M. Yoshida, S. Masaoka, K. Sakai, *Chem. Lett.* **2009**, *38*, 702–703; c) C. Casadevall, Z. Codolà, M. Costas, J. Lloret-Fillol, *Chem. Eur. J.* **2016**, *22*, 10111–10126.
[9] C. Casadevall, V. Martin-Diaconescu, W. R. Browne, S. Fernández, F. Franco, N. Cabello, J. Benet-Buchholz, B. Lassalle-Kaiser, J. Lloret-Fillol, *Nat. Chem.* **2021**, *13*, 800–804.
[10] a) N. Planas, L. Vigara, C. Cady, P. Miró, P. Huang, L. Hammarström, S. Styring, N. Leidel, H. Dau, M. Haumann, L. Gagliardi, C. J. Cramer, A. Llobet, *Inorg. Chem.* **2011**, *50*, 11134–111342; b) Y. Pushkar, D. Moonshiram, V. Purohit, L. Yan, I. Alperovich, *J. Am. Chem. Soc.* **2014**, *136*, 11938–11945; c) L. Yan, R. Zong, Y. Pushkar, *J. Catal.* **2015**, *330*, 255–260; d) Q. Daniel, P. Huang, T. Fan, Y. Wang, L. Duan, L. Wang, F. Li, Z. Rinkevicius, F. Mamedov, M. S. G. Ahlquist, S. Styring, L. Sun, *Coord. Chem. Rev.* **2017**, *346*, 206–215; e) D. Erdman, Y. Pineda-Galvan, Y. Pushkar, *Catalysts* **2017**, *7*, 39–39; f) Y. Pineda-Galvan, A. K. Ravari, S. Shmakov, L. Lifshits, N. Kaveevivitchai, R. Thummel, Y. Pushkar, *J. Catal.* **2019**, *375*, 1–7; g) R. Ezhov, A. Karbakhsh Ravari, A. Page, Y. Pushkar, *ACS Catal.* **2020**, *10*, 5299–5308; h) D. Lebedev, Y. Pineda-Galvan, Y. Tokimaru, A. Fedorov, N. Kaeffer, C. Copéret, Y. Pushkar, *J. Am. Chem. Soc.* **2017**, *140*, 451–458; i) M. Gil-Sepulcre, J. O. Lindner, D. Schindler, L. Velasco, D. Moonshiram, O. Rüdiger, S. DeBeer, V. Stepanenko, E. Solano, F. Würthner, A. Llobet, *J. Am. Chem. Soc.* **2021**, *143*, 11651–11661.
[11] a) J. L. Cape, S. V. Lymar, T. Lightbody, J. K. Hurst, *Inorg. Chem.* **2009**, *48*, 4400–4410; b) D. Moonshiram, J. W. Jurss, J. J. Concepcion, T. Zakharova, I. Alperovich, T. J. Meyer, Y. Pushkar, *J. Am. Chem. Soc.* **2012**, *134*, 4625–4636; c) D. Moonshiram, I. Alperovich, J. J. Concepcion, T. J. Meyer, Y. Pushkar, *Proc. Natl. Acad. Sci. USA* **2013**, *110*, 3765–3770.
[12] A. C. Dengel, W. P. Griffith, *Inorg. Chem.* **1991**, *30*, 869–871.
[13] J. Amtawong, D. Balcells, J. Wilcoxen, R. C. Handford, N. Biggins, A. I. Nguyen, R. David Britt, T. Don Tilley, *J. Am. Chem. Soc.* **2020**, *141*, 9859–19869.
[14] a) A. J. Wain, R. G. Compton, R. Le Roux, S. Matthews, K. Yunus, A. C. Fisher, *J. Phys. Chem. B.* **2006**, *110*, 26040–26044; b) S. Neukermans, J. Hereijgers, H. Y. Vincent Ching, M. Samanipour, S. Van Doorslaer, A. Hubin, T. Breugelmans, *Electrochem. Commun.* **2018**, *97*, 42–45.
[15] R. Stösser, U. Marx, W. Herrmann, J. K. Jabor, A. Brückner, *J. Am. Chem. Soc.* **2010**, *132*, 9873–9880.

Manuscript received: September 17, 2021
Revised manuscript received: November 12, 2021
Accepted manuscript online: November 17, 2021